Source contribution analysis of PM$_{2.5}$ using Response Surface Model and Particulate Source Apportionment Technology over the PRD region, China

Zhifang Li [a], Yun Zhu [a,*], Shuxiao Wang [b], Jia Xing [b], Bin Zhao [b], Shicheng Long [c], Minhui Li [d], Wenwei Yang [c], Ruolin Huang [a], Ying Chen [a]

[a] Guangdong Provincial Key Laboratory of Atmospheric Environment and Pollution Control, College of Environment and Energy, South China University of Technology, Guangzhou Higher Education Mega Center, Guangzhou 510006, China
[b] State Key Joint Laboratory of Environment Simulation and Pollution Control, School of Environment, Tsinghua University, Beijing 100084, China
[c] Guangzhou Urban Environmental Cloud Information Technology R&D Co. Ltd, Guangzhou 510006, China
[d] Guangdong Provincial Academy of Environmental Science, Guangzhou 510006, China

HIGHLIGHTS

- PM$_{2.5}$ source contributions are comparatively analyzed using RSM and PSAT.
- Both RSM and PSAT can reasonably assess the primary PM$_{2.5}$ emission contributions.
- PSAT has the limitation of quantifying the nonlinear contributions to secondary PM$_{2.5}$.
- RSM can well capture the PM$_{2.5}$ disbenefits by local NO$_x$ emission reductions.
- Dust and mobile sources are two major contribution sectors to PM$_{2.5}$ in PRD, China.

GRAPHICAL ABSTRACT
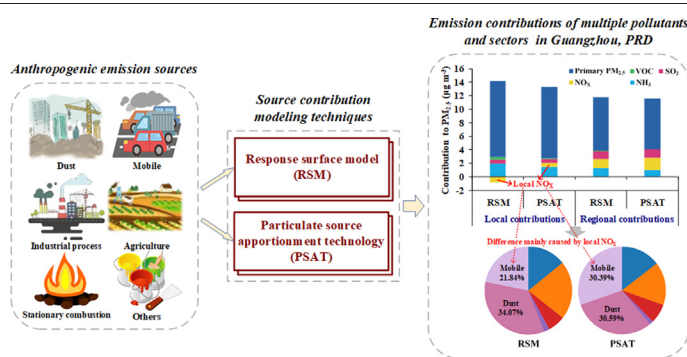
ARTICLE INFO

ABSTRACT

Identifying the emission source contributions to PM$_{2.5}$ is essential for a sound PM$_{2.5}$ pollution control policy. In this study, we conduct a comparative analysis of PM$_{2.5}$ source contributions over the Pearl River Delta (PRD) region of China using two advanced source contribution modeling techniques: Response Surface Model (RSM) and Particulate Source Apportionment Technology (PSAT). Our comparative analyses show that RSM and PSAT can both reasonably predict the contribution of primary PM$_{2.5}$ emission sources to PM$_{2.5}$ formation due to its linear nature. For the secondary PM$_{2.5}$ formed by the nonlinear reactions among PM$_{2.5}$ precursors, however, our study shows that PSAT appears to have limitations in quantifying the nonlinear contribution of PM$_{2.5}$ precursors to emission reductions, while RSM seems to better address the nonlinear relationship among PM$_{2.5}$ precursors (e.g., PM$_{2.5}$ disbenefits due to local NO$_x$ emission reductions in major cities with high NO$_x$ emissions). The pilot study case results show that for the ambient PM$_{2.5}$ in the central cities (Guangzhou, Shenzhen, Foshan, Dongguan, and Zhongshan) of the PRD, the regional source emissions contribute the most by 42–66%; the dust emissions are the top contribution sources (29–34% by RSM and 27–31% by PSAT), and the mobile sources are listed as the secondary contributors accounting for 16–25% by RSM and 19–30% by PSAT among the

* Corresponding author.
  E-mail address: zhuyun@scut.edu.cn (Y. Zhu).

anthropogenic emission sources. The city-scale cooperation on emission reductions and the enhancement of dust and mobile emission control are recommended to effectively reduce the ambient $PM_{2.5}$ concentration in the PRD.

1. Introduction

The Pearl River Delta (PRD) region of China has made great achievements in alleviating the $PM_{2.5}$ pollution in recent years, with the annual mean $PM_{2.5}$ concentration over the PRD decreasing by 51% between 2013 and 2020 (Fig. S1). However, in the years from 2015 to 2019, the overall decreasing tendency is slow with an annual decline less than 7% in the PRD. Influenced by COVID-19 (GDEEP, 2021), $PM_{2.5}$ in the PRD decreases by 25% in 2020, with the concentration sharply dropping to 21 µg m^{-3}. Based on the $PM_{2.5}$ concentration (e.g., 21 µg m^{-3} averaged over the PRD) in 2020, the China's 14th Five-Year Plan (2021–2025) (China, 2021) further proposes a challengeable $PM_{2.5}$ reduction rate target of 10% by the end of 2025 compared to 2020. Therefore, identifying the emission sources with the largest contributions to ambient $PM_{2.5}$, and then formulating a sound $PM_{2.5}$ pollution control strategy is still listed as one of the priority tasks in the PRD.

The $PM_{2.5}$ source contributions are mainly analyzed based on two kinds of modeling approaches, the monitoring-based receptor models and the modeling-based 3-dimensional air quality models (3-D AQMs) (Wang et al., 2016; Xie et al., 2016). The receptor models, including chemical mass balance (CMB) (Watson et al., 1984), positive matrix factorization (PMF) (Paatero and Tapper, 1994), and principal component analysis (PCA) (Belis et al., 2013), can assess the source contributions by matching common characteristics between the source and receptor using statistical analysis approaches (Thunis et al., 2019). Receptor models have been extensively used for source contribution analysis because of their simple operation (Bi et al., 2011; Wang et al., 2009); nonetheless, they can hardly apportion the contributions of various emission sources to secondary pollutants and can also be effectively applied only in the proximity of a few specific monitoring sites (Li et al., 2018). Accordingly, the 3-D AQMs with the ability to identify the source contributions to secondary pollutants and assess the air quality at various spatial and temporal scales (Chen et al., 2018; Zhang et al., 2017), have become increasingly popular for $PM_{2.5}$ source contribution analysis (Zhu et al., 2018). There are mainly three types of source contribution analysis approaches based on the 3-D AQMs, including source sensitivity analysis method, tagged tracer technique, and response surface modeling technique (Pan et al., 2020; Thunis et al., 2019). Source sensitivity analysis method can quantify the sensitivities of pollutant concentrations to changes in model input parameters (e.g., emissions), in which the brute force method (BFM) is the simplest approach that can directly acquire the sensitivity coefficients by perturbing the input parameters individually (Huang et al., 2018; Yamaji et al., 2012). A more advanced decoupled direct method (DDM) is also proposed to provide information about the sensitivities by solving sensitivity equations decoupled from the model equations (Dunker, 1984; Ivey et al., 2015); a higher-order DDM (HDDM) is further developed to obtain the sensitivities under the nonlinearity through calculating the higher-order derivatives of first-order equations (Hakami et al., 2003, 2004). The tagged tracer technique, which can apportion the source contributions by tracking multiple reactive tracer species in a single model run (Dunker et al., 2002), is available for allocating the contributions of various source groups (i.e., different source regions and categories) to target pollutant concentrations. The Particulate Source Apportionment Technology (PSAT) within the Comprehensive Air Quality Model with Extensions (CAMx) (Chen et al., 2019; Kim et al., 2017; Li et al., 2015; Lu et al., 2019; Wang et al., 2017) and the Integrated Source Apportionment Model (ISAM) within the Community Multi-scale Air Quality model (CMAQ) (Byun and Schere, 2006; Chang

et al., 2019; Chen et al., 2017; Foley et al., 2010; Napelenok et al., 2014) are the two most commonly used tagged tracer techniques nowadays. The Response Surface Model (RSM) with the ability to predict the response of pollutant concentrations under different emission control scenarios in real time (Jin et al., 2020; Xing et al., 2011, 2018, 2019, 2020a,b; Zhao et al., 2015), has also been applied for source contribution analysis (Fang et al., 2020; Pan et al., 2020). RSM is a reduced-form meta-model that is constructed by fitting multiple AQM simulations using statistical algorithms. Compared with DDM, which is not suitable for quantifying sensitivities under large emission perturbations in the nonlinear system (Itahashi et al., 2015; Koo et al., 2009; Zhang et al., 2005), RSM has been proven to provide more accurate response predictions to large emission cuts and well capture nonlinear characteristics (Foley et al., 2014). Although the aforementioned techniques based on the 3-D AQMs have been previously employed for source contribution analysis, the underlying mechanisms of the individual approaches are essentially different (Clappier et al., 2017; Thunis et al., 2019). Identifying the consistency and inconsistency between different source contribution analysis methods can not only provide insights into the strengths and limitations of each method, but also favor illustrating the capability of each method in air quality management applications. Several studies have been conducted to evaluate the similarities and discrepancies among different modeling approaches for $PM_{2.5}$ source contribution analysis (Burr and Zhang, 2011b; Chatani et al., 2020; Foley et al., 2014; Koo et al., 2009), but there is barely a comparative analysis based on the RSM and other methods (e.g., PSAT).

Therefore, this study aims to comprehensively evaluate the $PM_{2.5}$ source contributions over the PRD region of China using RSM and PSAT, analyze the corresponding consistency and inconsistency between the two methods, and explore the possible causes for the discrepancies between. Based on the source contribution results derived from RSM and PSAT, the emission control policy for effectively reducing the ambient $PM_{2.5}$ levels in the PRD is also recommended.

2. Methodology

The emission source contributions to $PM_{2.5}$ over the PRD region are comprehensively analyzed (Fig. 1). Firstly, the modeling systems of Weather Research and Forecasting-CMAQ (WRF-CMAQ) and WRF-CAMx are run respectively based on the same input of meteorology and emissions. Secondly, the CMAQ is used to simulate the $PM_{2.5}$ concentrations over the PRD in 2017 under the designed control matrices, which consist of various control scenarios parameterized by different emission control variables (i.e., pollutants, regions, and sectors). Then, the RSM with differential method (DM) (Pan et al., 2020) is established based on the CMAQ simulations. Thirdly, the multiple tracer species corresponding to the emission control variables are selected and then added to CAMx's built-in PSAT to track the source regions and sectors of $PM_{2.5}$. Finally, the individual emission sector contribution and the contributions of multiple pollutants, regions, and sectors to $PM_{2.5}$ in receptors are comprehensively evaluated by RSM and PSAT.

2.1. Model configurations

The nested modeling domain setting is shown in Fig. 2, and the horizontal resolutions for domain 01 (d01), domain 02 (d02), and domain 03 (d03) are 27 km, 9 km, and 3 km, respectively. The d03 domain, which covers the entire PRD region, is divided into Guangzhou (GZ),
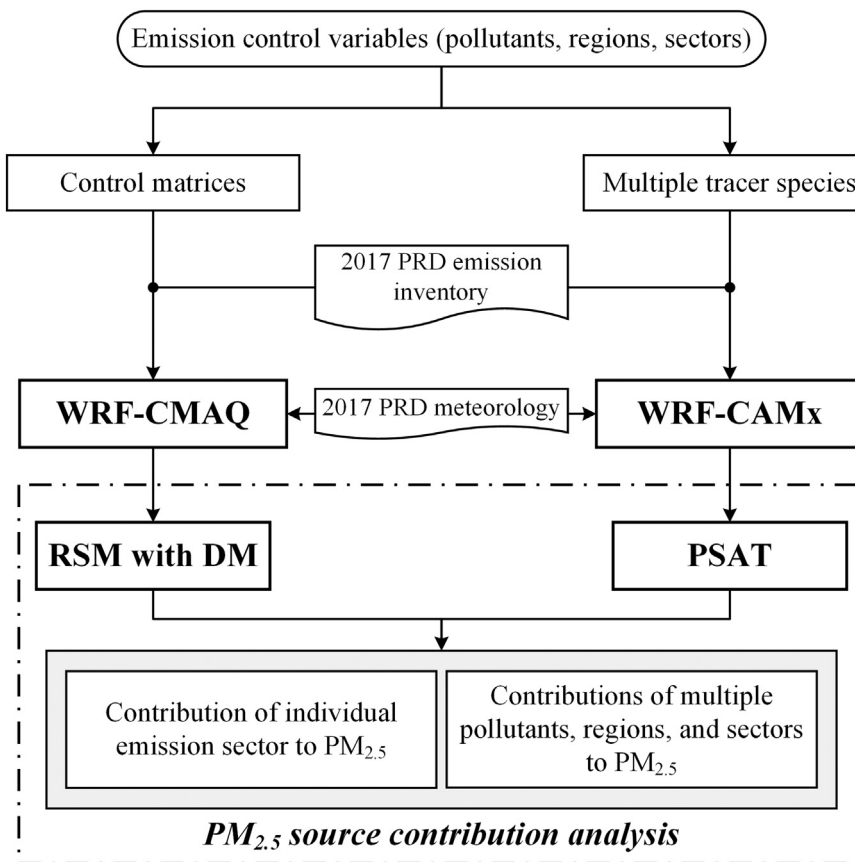
Fig. 1. The process for analyzing the source contributions to $PM_{2.5}$ over the PRD region using RSM and PSAT.

Shenzhen (SZ), Foshan (FS), Dongguan (DG), Zhongshan (ZS), and other regions (OTH). The assessments of source contribution comparison are conducted in the d03 domain.

The WRF version 3.9.1 is used for the meteorology field simulation and the CMAQ version 5.2 and CAMx version 7.0 are applied to simulate the $PM_{2.5}$ concentration. The simulation period is January 2017 because
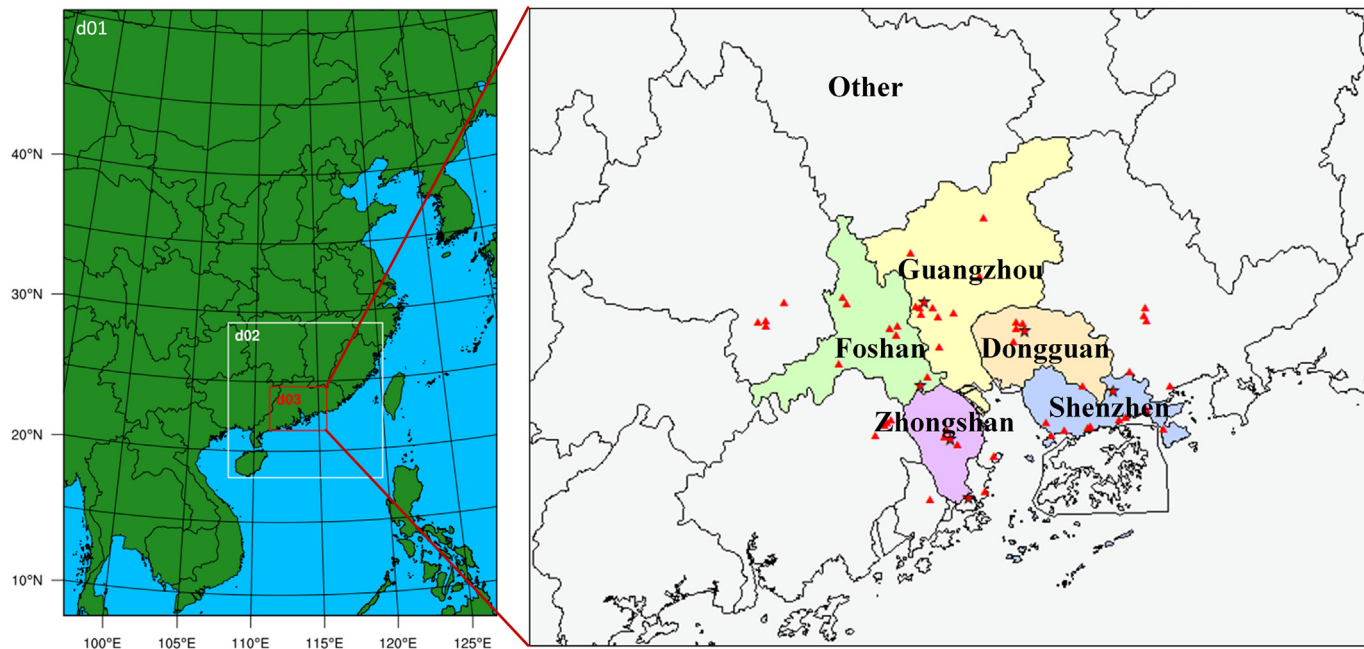

Fig. 2. Simulation domain and national-controlled air-monitoring sites in the PRD region (Red triangles: monitor sites; Red pentacles: monitor sites selected to evaluate the model performance of CMAQ and CAMx). (For interpretation of the references to color in this figure legend, the reader is referred to the web version of this article.)

of the relatively high ambient $PM_{2.5}$ concentration in the PRD in the whole year of 2017 (HKEPD, 2018). The model configurations for WRF are shown in Table S1 and those for CMAQ and CAMx (Table S2) are set similarly to minimize differences. For example, the Carbon Bond version 6 (CB6) is chosen for gas-phase chemistry in CMAQ and CAMx, and the aerosol chemistry is represented by the AERO6 and the coarse-fine scheme version 2 (CF2) in CMAQ and CAMx, respectively. The initial and boundary conditions stem from the CMAQ simulations and are prepared for CAMx using the Cmaq2camx processor; the spin-up time for CMAQ and CAMx models is 5 days.

For the outer and middle domains, the 2017 anthropogenic emission inventories provided by Tsinghua University are implemented (Zheng et al., 2018). For the innermost domain, the 2017-based PRD regional emission inventory is applied (Fang et al., 2021). The biogenic emissions are prepared from the Model of Emissions of Gases and Aerosols from Nature (MEGAN) version 2.1 (Guenther et al., 2012).

2.2. Response surface modeling technology

RSM is a meta-model built upon CMAQ simulations with the capability of predicting the real-time response of pollutant concentrations to emission source perturbations. In this study, the new polynomial functions-based extended RSM coupled with the sectoral linear fitting technique developed by Pan et al. (2020), is utilized to effectively quantify the nonlinear response of air pollutant concentrations to precursor emission changes from multiple source regions and sectors. The development of the new RSM is detailed in Pan et al. (2020).

The specific experiment design for constructing and validating the RSM in our study is summarized in Table S3, and the corresponding detailed control matrices are shown in Fig. S2. In general, there are three steps to construct the RSM. First, the relationship between the $PM_{2.5}$ response in receptor regions to total precursor (i.e., NO_x, SO_2, VOC, and NH_3) emission changes from multiple source regions is fitted by a series of polynomial functions (Xing et al., 2017, 2018; Zhao et al., 2015). For this, a total of 141 emission control scenarios simulated by CMAQ are required, including one base scenario, 120 scenarios for establishing the $PM_{2.5}$ response in each receptor region to changes in total precursor emissions from each source region (i.e., 20 scenarios for each receptor region), and 20 scenarios for creating the $PM_{2.5}$ response in each receptor region to simultaneous changes in total precursor emissions from all source regions. Second, the linear relationship between total precursor emissions from all sectors and precursor emissions from individual sectors in each source region is established by 169 emission control scenarios (i.e., 28 scenarios for each source region in addition to one base scenario) (Cohan et al., 2005; Pan et al., 2020). The total emissions of each precursor from each source region are classified into those from 6 sectors, including industrial process, mobile, stationary combustion, agriculture, dust, and other sources (including solvent use, fuel oil storage, waste treatment, biomass burning, and catering). Then, the relation of the $PM_{2.5}$ response in each receptor region to multiregional and multisectoral precursor emission changes can be established based on the first two steps. Third, the relationship between the $PM_{2.5}$ response to primary $PM_{2.5}$ emission changes from multiple regions and sectors is fitted by 37 emission control scenarios using the linear function (i.e., 6 scenarios for each receptor region in addition to one base scenario) (Long et al., 2016). The primary $PM_{2.5}$ emission sources from each source region are also categorized into 6 sectors as mentioned before. In addition, the extra 30 emission control scenarios randomly generated by Hamersley quasi-random Sequence Sampling (HSS) between 0 and 1.5 (base scenario = 1) are used for out-of-sample (OOS) validation to assess the performance of the established RSM (Wang et al., 2011; Xing et al., 2011, 2017, 2018; Zhao et al., 2015, 2017).

Based on the constructed RSM, various emission source contributions to $PM_{2.5}$ can be evaluated. For estimations of individual source contributions, the employed RSM mechanism is identical to the traditional BFM in air quality models. For assessments of multiple source contributions, the innovative DM within the RSM is applied to calculate the contributions by dividing the emission changes into a range of tiny sections and summing up the $PM_{2.5}$ response corresponding to each tiny change. By the division into tiny intervals, RSM with DM can ensure the $PM_{2.5}$ response to changes in its precursor emissions is linear in each interval, which can not only catch the negative contribution but also ensure that the accumulative responses are consistent with the total contribution stemming from the CMAQ integrated scenario. More details about the development of DM are described in Pan et al. (2020).

2.3. Particulate Source Apportionment Technology

PSAT is an extension tool of CAMx that can track the source regions and source categories of primary and secondary $PM_{2.5}$ species in every grid cell using the reactive tracer technique (Wu et al., 2013). For the primary $PM_{2.5}$ species tracked, only a single tracer family is required, but for the secondary $PM_{2.5}$ species, several tracer families are needed to track the relationship between precursors and the resulting $PM_{2.5}$ compounds. The PSAT splits the $PM_{2.5}$ concentration into a sum of contributions, each related to a specific emission source (Thunis et al., 2019). Especially for the secondary compounds, the decomposition is conducted by attributing the concentration of each part of the compounds (e.g., NO_3, SO_4, and NH_4) to its directly related precursor (e.g., NO_2, SO_2, and NH_3) (Thunis et al., 2018). Although this decomposition is arbitrary because it depends on the chemical pathway selection and the relative weights for splitting the secondary compounds, it can ensure that the sum of contributions equals the modeled $PM_{2.5}$ concentration (Kranenburg et al., 2013). More details about PSAT can be found in the CAMx manual (http://www.camx. com/). In this study, the anthropogenic emission inventory of the d03 domain applied in PSAT is mainly divided into 6 sectors following the treatment of RSM.

3. Results and discussion

3.1. Model performance

The performance of WRF is verified based on the hourly meteorological observations from the central monitor site (Shundesugang site in FS) of the d03 domain. The validation results of temperature, wind speed, and relative humidity in January 2017 are summarized in Table S4. Overall, the simulation results of WRF are acceptable for further application in the CMAQ and CAMx models. In detail, the simulated temperature and relative humidity perform well with Correlation coefficients (R) above 0.88, Indices of Agreement (IOAs) above 0.93, and Normalized Mean Biases (NMBs) within ±4%. The wind speed is overestimated by WRF (NMB, 98.18%), which is also found in our previous studies (Fang et al., 2021; Huang et al., 2020; Pan et al., 2020) and other researches (Huang et al., 2018; Liu et al., 2020). This overestimation of wind speed has always existed from the early to current versions of the WRF and is mainly due to the exclusion of urban canopy from WRF (Jiménez and Dudhia, 2012; Santos-Alamillos et al., 2015). Though the wind speed is overpredicted, the model still reasonably simulates the wind evolutionary characteristics. For instance, the Root Mean Squared Error (RMSE) of wind speed is close to the observed value, with R (0.75) and IOA (0.60) acceptable (Huang et al., 2018).

Comparing the CMAQ-simulated and CAMx-simulated $PM_{2.5}$ concentrations in January with the observations at 6 national controlled air quality monitoring sites selected in 6 target regions (including Luhu site in GZ, Longgang site in SZ, Rongguijiedaoban site in FS, Dongchengshijing site in DG, Zimaling site in ZS, and Qianshan site in OTH), the performance of CMAQ and CAMx is evaluated. According to the hourly time series comparisons of the observed data and simulated results shown in Fig. S3a, both CMAQ and CAMx can reasonably

simulate the temporal variation and magnitude of $PM_{2.5}$, with R ranging from 0.68 to 0.72 for CMAQ, from 0.66 to 0.69 for CAMx, and NMB ranging from −8.20% to 4.51% for CMAQ, from −5.68% to 3.87% for CAMx, respectively. These NMBs well meet the criteria of NMB < ±30% recommended by Emery et al. (2017). Moreover, there is a good agreement between the $PM_{2.5}$ concentrations predicted by the CMAQ and CAMx, with R values being larger than 0.87 (Fig. S3b). Additionally, Fig. S4 presents the comparison of the monthly mean $PM_{2.5}$ concentrations simulated by CMAQ and CAMx over all grid cells of the PRD under the base case and scenario with 100% control of all key sector emissions, and also the delta scenario between the base and control scenario. Similar to that in the base case simulation (R equals to 0.99), the two models agree well on the control scenario related to the source apportionment (R equals to 0.94 for control scenario and 0.99 for delta scenario). The small differences between the simulation results of the two models, which are inevitably caused by the different chemistry schemes, dry and wet deposition modules, and PM size representations in the host models, ensure that the differences in subsequent source contribution analysis results are primarily attributed to discrepancies in source contribution analysis approaches rather than discrepancies in underlying models (Burr and Zhang, 2011b; Fang et al., 2021). Overall, both the WRF-CMAQ and WRF-CAMx modeling systems can reasonably simulate the meteorological fields and capture the $PM_{2.5}$ concentration well.

Referring to the statistical indices used for OOS validation in Pan et al. (2020), the average Mean Square Error (aMSE), average RMSE (aRMSE), average Relative Root Mean Squared Error (aRRMSE), average and maximum Mean Normalized Error (aMNE and maxMNE), and average R (aR) are selected to quantitatively assess the reliability of RSM by comparing the RSM-predicted and corresponding CMAQ-simulated $PM_{2.5}$ concentrations for the 30 OOS control scenarios. The comparison results summarized in Table S5 show that the $PM_{2.5}$ concentrations in January simulated by CMAQ can be well reproduced by RSM with aMSE of 0.01–0.08 $\mu g\ m^{-3}$, aRMSE of 0.07–0.25 $\mu g\ m^{-3}$, aRRMSE of 0.23–0.89%, aMNE of 0.06–0.44%, and aR of almost 1. Even in the case with maximal MNE from the OOS case 11–20, RSM can also predict the quite similar spatial distribution of $PM_{2.5}$ concentration as that of CMAQ (Fig. S5), with their delta (RSM minus CMAQ) in the range −0.92 to 3.67 $\mu g\ m^{-3}$ over the entire domain. Taken together, the overall performance of RSM established in this study is comparable to those in previous publications (Pan et al., 2020; Xing et al., 2018).

3.2. Comparison of source contributions between RSM and PSAT

3.2.1. Analysis of contribution of individual emission sector to $PM_{2.5}$

The contributions of individual emission sector to $PM_{2.5}$ concentrations are analyzed by the RSM and PSAT over the PRD region in January, and the corresponding BFM results based on the CMAQ simulations are chosen as standards to evaluate the performance of RSM and PSAT as in previous studies (Itahashi et al., 2015; Koo et al., 2009). As shown in Figs. 3 and S6, the contribution to $PM_{2.5}$ estimated by the BFM, RSM, and PSAT for each emission sector are fairly similar in terms of the spatial distributions, although the relative magnitudes predicted by these three methods are different to a certain extent.

For industrial process emissions, BFM, RSM, and PSAT results are almost consistent in space, with the largest contributions occurring over the Foshan (Fig. 3a). However, PSAT tends to give slightly higher contributions to the grids in Foshan while the RSM nearly reproduces the BFM results (Fig. S6a). For example, the maximum contribution to the grids in Foshan estimated by the BFM and RSM is 71.04 $\mu g\ m^{-3}$ and 70.03 $\mu g\ m^{-3}$ respectively, while that estimated by the PSAT is 79.18 $\mu g\ m^{-3}$. The higher estimation by PSAT is due to two factors. First, the industrial process sources in Foshan emit a relatively high level of NO_x (Table S7); therefore, the elimination of industrial process emissions reduces the NO_x concentrations, which results in the increased availability of oxidants for the oxidation of SO_2 in the atmosphere (Burr and Zhang, 2011a; Fang et al., 2020, 2021). Second,

reducing NO_x concentrations slightly decreases the production of nitric acid, which in turn lowers the acidity of the aqueous phase under winter conditions and leaves more SO_2 to be dissolved and oxidized in the aqueous phase (Koo et al., 2009). These indirect effects of increased sulfate concentrations somewhat offset the overall $PM_{2.5}$ decrease caused by the industrial process NO_x emission reductions. However, because PSAT neglects these indirect effects and is designed to link each secondary $PM_{2.5}$ compound only to its direct primary precursor (e.g., the sulfate is only linked to SO_2), the source contribution from NO_x is significantly overestimated by PSAT in winter.
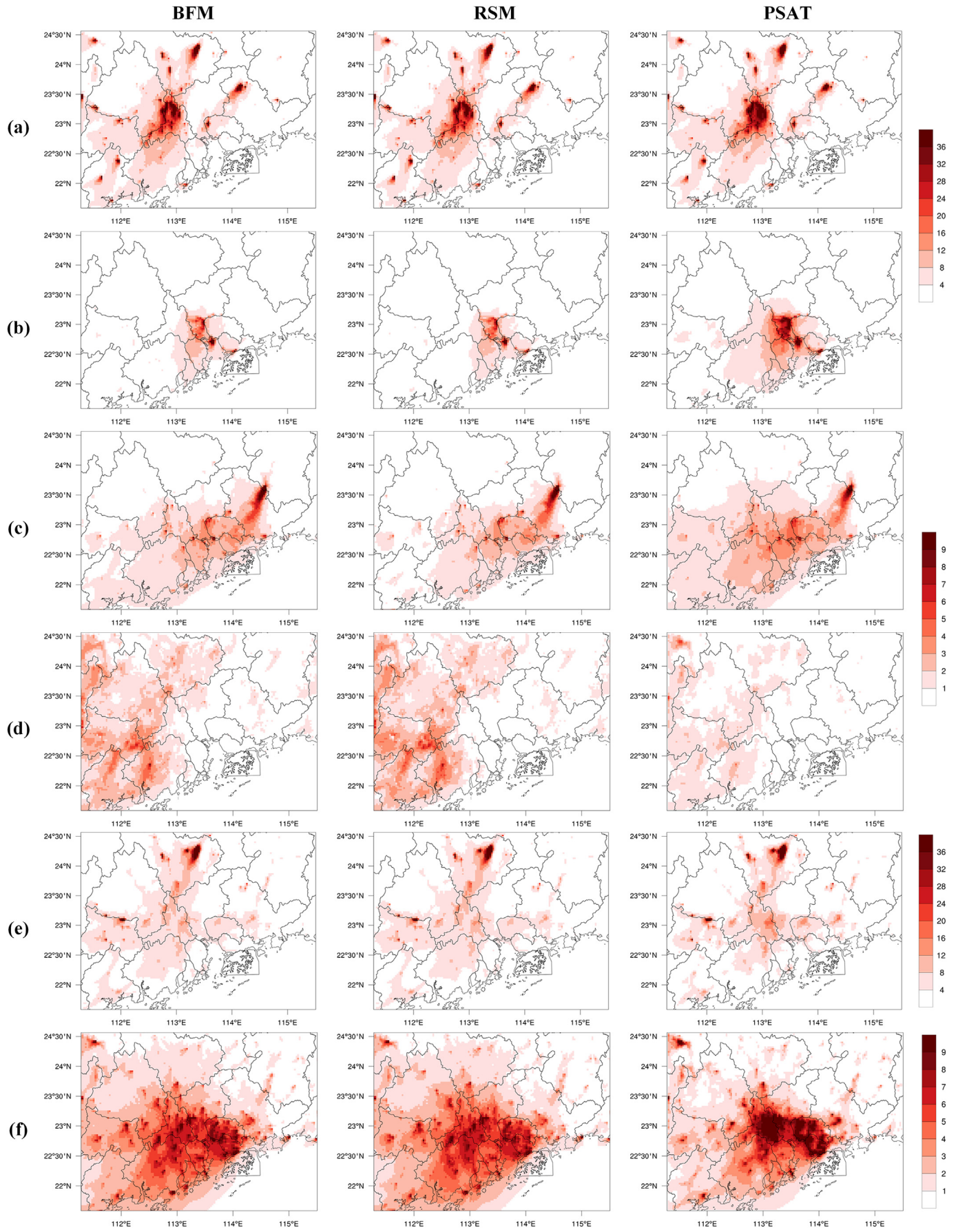
For mobile emissions, the contributions and the most affected regions estimated by BFM and RSM are quite consistent spatially, while both the magnitudes and range of affected areas produced by PSAT are larger than BFM (Figs. 3b and S6b). In particular, in the urban areas of Guangzhou where the total possession of vehicles is large, the largest difference between BFM and PSAT is approximately up to 8.38 $\mu g\ m^{-3}$, while there is only a slight difference of 0.1 $\mu g\ m^{-3}$ between BFM and RSM. These differences between PSAT and BFM are also primarily caused by the indirect contributions from an increase in sulfate concentrations caused by the NO_x emission reductions, as the NO_x emissions are dominated by mobile sources in the PRD, particularly in Guangzhou (Tables S6 and S7) (Fang et al., 2020, 2021; Pan et al., 2020).

A similar phenomenon is observed in the assessments for stationary combustion emission contributions among the BFM, RSM, and PSAT. Good agreement is found between the RSM and BFM for contributions to $PM_{2.5}$ concentrations from stationary combustion emissions, while the PSAT still gives slightly higher contributions than BFM over part of the domain (Figs. 3c and S6c). This is also mainly attributed to the aforementioned indirect effects of NO_x emission reductions on sulfate because of the relatively high NO_x emissions from stationary combustion in the PRD (Table S6).

For agriculture emissions, the $PM_{2.5}$ contributions predicted by PSAT are lower than BFM (Fig. 3d), particularly in the regions where agricultural activities are high (e.g., Jiangmen), the maximum difference between PSAT (2.44 $\mu g\ m^{-3}$) and BFM (7.18 $\mu g\ m^{-3}$) is 4.74 $\mu g\ m^{-3}$ (66%) (Fig. S6d). Yet the overall deviation of RSM results from those of BFM is small spatially, and their differences are within ±1 $\mu g\ m^{-3}$ across the entire domain (Fig. S6d). Reductions in NH_3 emissions from agriculture can limit the formation of ammonium sulfate and ammonium nitrate, resulting in a significant decrease in NO_3^- and SO_4^{2-} in January (Fu et al., 2017). The effects of reduced NH_3 emissions on nitrate and sulfate in winter are taken into account by RSM but ignored by PSAT, causing the underestimation of PSAT and the good agreement of RSM compared with the BFM.

Since $PM_{2.5}$ concentrations are linearly related to primary $PM_{2.5}$ emissions, the dominant component of dust sources (Table S6), the three approaches give quite similar results for dust emissions (Figs. 3e and S6e). The relatively good agreements in primary $PM_{2.5}$ contributions among the three methods further illustrate that differences in source contribution results are mostly originating from the source contribution analysis methods rather than the host models. For the emission sources other than those discussed above (including solvent use, fuel oil storage, waste treatment, biomass burning, and catering), relatively large discrepancies appear in spatial distributions (Fig. 3f) and magnitudes (Fig. S6f) between BFM and PSAT. It may also be attributed to the complex interactions of various emission species contained, though they agree that the largest contributions occur in the central cities of the PRD (e.g., Guangzhou, Shenzhen, Foshan, Dongguan). The RSM results are fairly consistent with BFM both in space and magnitudes (Figs. 3f and S6f).

Additionally, in China, the attainment of air quality standards in regions and the efficiency of formulated control strategies are mainly measured by the air quality of national-controlled air-monitoring local sites. Therefore, the $PM_{2.5}$ contribution results obtained from the BFM, RSM, and PSAT at all national-controlled air-monitoring sites of the
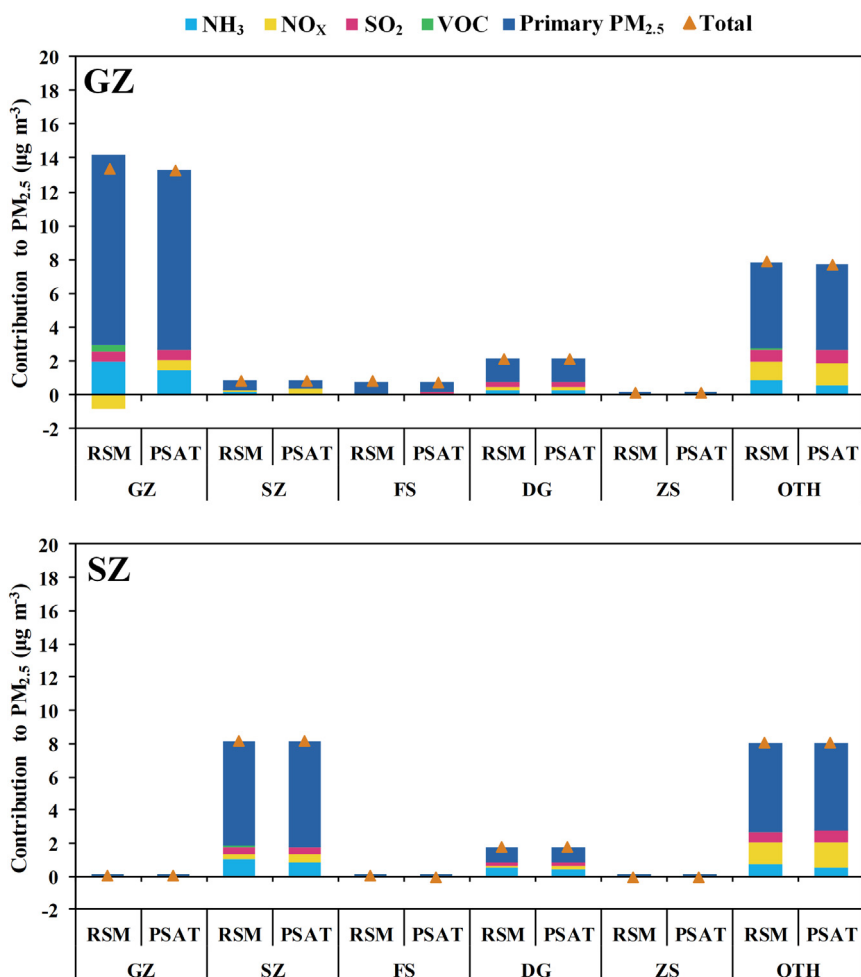
Fig. 4. Comparison of the contributions to monthly mean PM$_{2.5}$ concentrations in GZ and SZ from different source regions and pollutants in January (RSM results are generated by a 100% reduction in all emissions, and the colored bar denotes the contribution only from the pollutant's own emission change; Brownish triangle: total contribution of all pollutant emissions from each source region; GZ: Guangzhou, SZ: Shenzhen, FS: Foshan, DG: Dongguan, ZS: Zhongshan, OTH: all the other areas in the d03 domain). (For interpretation of the references to color in this figure legend, the reader is referred to the web version of this article.)

PRD in January are further compared through scatter plots (Fig. S7). Similar conclusions to the spatial distribution comparisons are also drawn from the scatter plots. For example, as revealed by the regression slopes between the results of PSAT versus BFM and RSM versus BFM, PSAT attributes greater importance (slopes > 1) to industrial process, mobile, and other sources emissions than BFM, whereas RSM nearly replicates the BFM results (slopes are almost equal to 1). For dust emissions, the PSAT and RSM both agree reasonably well with the BFM (slopes equal to 1), but the agreement between PSAT and BFM is slightly less perfect than that of RSM. This slight deviation in primary PM$_{2.5}$ contributions between PSAT and BFM indicates that different host models do inevitably bring some differences in source contribution analysis results, but the effect of these differences is not significant in this study (Burr and Zhang, 2011b). Moreover, the correlations between RSM and BFM ($R > 0.94$) are generally better than those between PSAT and BFM ($R > 0.89$) for all emission sectors. Although the disagreement in magnitudes of PSAT and RSM results is relatively large (except stationary combustion and dust), there is still a good correlation between them, with R values being larger than 0.93 (except agriculture).

3.2.2. Analysis of contributions of multiple pollutants, regions, and sectors to PM$_{2.5}$

To evaluate the consistency and complementarity in multiple source contributions between the RSM and PSAT, the emission contributions of pollutants from different source regions to monthly mean PM$_{2.5}$ concentrations are first systematically estimated in 5 central cities of the PRD (i.e., GZ, SZ, FS, DG, and ZS) (Figs. 4 and S8). The results for each city are calculated on the basis of all local national-controlled air-monitoring sites in the city, and the RSM results are generated by DM under the 100% control scenario for all emissions. As demonstrated in Figs. 4 and S8, both RSM and PSAT agree that the primary PM$_{2.5}$ emissions are the most important contributors to PM$_{2.5}$ concentrations in 5 receptor cities, particularly those from local emissions, significantly contributing 27–49% (by RSM) and 27–48% (by PSAT). Good agreement between RSM and PSAT is also found in the total local (i.e., contributions from receptor region itself) and regional contributions (i.e., contributions from other source regions except receptor region in the d03 domain) of all precursors (i.e., the sum of SO$_2$, VOC, NH$_3$, and NO$_x$). Taking GZ and SZ as examples (Fig. 4), the

Fig. 3. Spatial distribution of PM$_{2.5}$ source contributions calculated by BFM, RSM, and PSAT respectively for emissions from (a) industrial process, (b) mobile, (c) stationary combustion, (d) agriculture, (e) dust, and (f) other sources in January (unit: μg m^{-3}; RSM and BFM results are generated by a 100% reduction in individual emission sectors).

total contributions of all precursors from regional transport are larger than those from local emissions.

While RSM and PSAT give the most consistent estimations for the local and regional primary PM$_{2.5}$ emissions due to the linear processes of primary PM$_{2.5}$ emissions, their predictions for precursors differ to varying degrees. For SO$_2$ emissions, the RSM's and PSAT's calculations are quite similar as a result of the relatively small nonlinear interactions between the SO$_2$ emissions and sulfate formation in winter (Itahashi et al., 2017). The slightly higher contribution estimations of SO$_2$ by PSAT than RSM are possibly due to the indirect effects accounted for in RSM but not in PSAT, in which the elimination of SO$_2$ emissions can make more oxidants accessible for the oxidation of other precursors (e.g., NO$_x$) and then slightly facilitate the formation of other secondary PM$_{2.5}$ compounds (e.g., nitrate) (Burr and Zhang, 2011b; Koo et al., 2009). RSM and PSAT agree that the contributions of VOC emissions to PM$_{2.5}$ are almost negligible in all receptors except for the local contributions in GZ, in which RSM's value is larger than PSAT's value. This is probably because PSAT overlooks the indirect influences of the VOC emission reductions on a slight decrease in NO$_3^-$ or SO$_4^{2-}$, which means that the reductions in VOC emissions can cause a decline in oxidants usable to oxidize NO$_x$ or SO$_2$ due to the reduced O$_3$ formation in GZ in winter (Fang et al., 2020). For NH$_3$ emissions, the contribution predictions of RSM are larger than those of PSAT in 5 receptor cities. One possibility for this result is that these central cities of the PRD are under NH$_3$-limited regime during the pollution period (Yin et al., 2018), and the NH$_3$ abatement can effectively lower the sulfate and nitrate concentrations, which are considered by RSM through the interaction terms in the polynomial functions but ignored by PSAT, making the relatively reasonable estimates for RSM. As for NO$_x$ emissions, the most obvious difference in contributions between RSM

and PSAT is that the RSM can predict the negative contributions of NO$_x$ emissions to PM$_{2.5}$, because NO$_x$ reductions result in more oxidants generated to oxidize other precursors (e.g., SO$_2$) (Fang et al., 2020; Thunis et al., 2021), causing the slight increase in secondary PM$_{2.5}$ (e.g., sulfate) concentrations consequently; whereas PSAT always predicts positive contributions. For instance, the local NO$_x$ contributions calculated by RSM in GZ and DG (Fig. S8) where the NO$_x$ emissions are high (Table S7) are -0.85 µg m^{-3} and -0.36 µg m^{-3}, while the contributions are 0.55 µg m^{-3} and 0.52 µg m^{-3} by PSAT, respectively. RSM is capable of capturing these nonlinear responses of secondary PM$_{2.5}$ to reductions in NO$_x$ emissions based on the polynomial functions; however, PSAT fails to identify them because it neglects these indirect effects and assumes no negative secondary PM$_{2.5}$ production for each source category (Burr and Zhang, 2011b).

Furthermore, the contributions of various source sectors to monthly mean PM$_{2.5}$ concentrations in 5 receptor cities are evaluated. It can be discerned from Figs. 5 and S9 that RSM and PSAT basically agree on the percentage contributions of 6 source sectors as well as their relative rankings in 5 receptor cities. In particular, the top two contributors identified by RSM and PSAT in each receptor are not only consistent in terms of source sectors, but also their total contributions explain more than 50% of the total PM$_{2.5}$ concentrations. For example, due to the large total possession of vehicles in GZ and SZ, the dust (road dust, construction dust, stockyard dust, etc.) and mobile sources are identified as the top two contributors by both RSM and PSAT in GZ and SZ, with a contribution of 29–34% and 22–25% (by RSM) and 30–31% and 26–30% (by PSAT) separately. In other 3 cities (i.e., FS, DG, and ZS; Fig. S9), the dust and mobile emissions are also the top and secondary contributors, accounting for 29–31% and 16–23% (by RSM) and 27–30% and 19–29% (by PSAT) respectively. These source contribution results are similar to
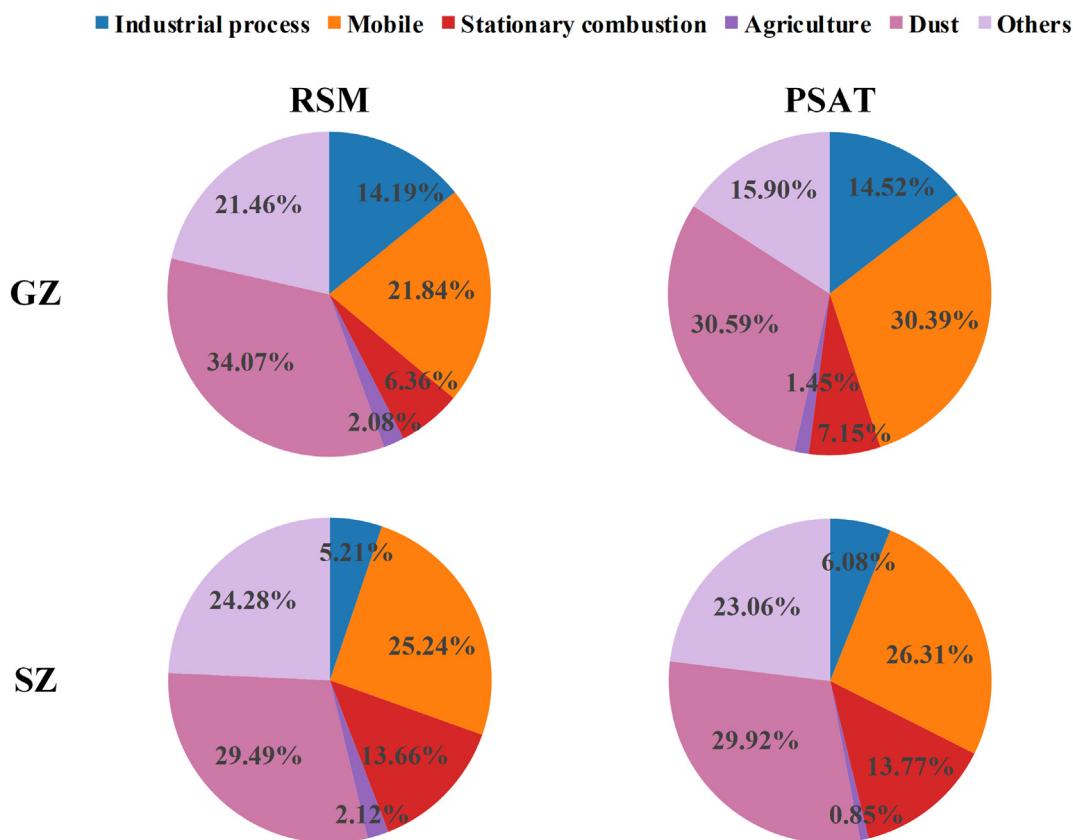

Fig. 5. Comparison of the percentage contributions to monthly mean PM$_{2.5}$ concentrations in GZ and SZ from different source sectors in January (RSM results are generated by a 100% reduction in all emissions; GZ: Guangzhou, SZ: Shenzhen).

those of other related researches in the PRD (Pan et al., 2020; Yang et al., 2020; Yin et al., 2017). Nevertheless, compared with the slight difference (PSAT minus RSM, 1%) in the contribution of mobile sources between RSM and PSAT in SZ, the difference in GZ is large (9%). It is because estimations in GZ are based on monitoring sites that are mainly located in the traffic volume network while those in SZ are close to the ocean. Intensive transportation can bring large amounts of NO_x emissions (Table S7), which means that the nonlinear effects of local NO_x emission reductions on $PM_{2.5}$ are stronger in GZ, leading to the higher difference between RSM and PSAT in GZ than in SZ.

The contributions of different source sectors from local emissions and regional transport to monthly mean $PM_{2.5}$ concentrations are also assessed in 5 receptor cities (Figs. 6 and S10), for which the estimates between RSM and PSAT for dust sources are the most similar. RSM and PSAT are consistent in source attribution results from local emissions (34–58%) and regional transport (42–66%) (Fig. S11), with differences lower than ±0.5%. For the local contributions of different source sectors to $PM_{2.5}$ in receptors, the dust emissions are determined as the most important sources by both RSM and PSAT, contributing 15–24% (by RSM) and 14–20% (by PSAT). Regardless of rankings, the other two major contributors assessed by both RSM and PSAT are mobile and other sources in GZ, SZ, DG, and ZS, but industrial process and other sources in FS. The largest deviation in local contributions of different source sectors between RSM and PSAT, about 8% (PSAT minus RSM, Fig. S11), is observed in the mobile sources in GZ, with a corresponding difference in the regional contribution of only 1%. For the regional contributions of various source sectors to $PM_{2.5}$ in receptors, some important results can be found. First, the most important regional

source estimated by RSM and PSAT for most receptors is consistent with each other. For example, in GZ, the most important regional source evaluated by RSM and PSAT is the industrial process (RSM, 12%; PSAT, 12%; Fig. S11). Second, the relative contribution and ranking of each source sector from each source region (except receptor region) estimated by RSM and PSAT at receptors are similar. Taking the contributions of each source sector from OTH to GZ as examples, both RSM and PSAT predict that industrial process emissions are most important sources, followed by dust emissions, mobile emissions, stationary combustion emissions, other sources emissions, and agriculture emissions. Third, the contribution from OTH is the largest for each receptor city. In addition to the OTH contribution, FS and ZS (Fig. S10), which are located downwind of the PRD under the prevailing northeasterly wind in January (Fig. S12), are significantly affected by the transportation of polluted air masses from upwind cities such as GZ, SZ, and DG. Among the contributions of various source sectors from these upwind cities, RSM and PSAT agree that the mobile sources from GZ contribute the most to FS and ZS. It may be attributed primarily to the considerable amounts of NO_x emitted from the mobile sources in GZ (Table S7) and the strong prevailing northeasterly wind that the NO_x from GZ can experience regional transportation and participate in chemical reactions in FS and ZS, aggravating the $PM_{2.5}$ pollution.

4. Conclusions

In this study, the source contributions to $PM_{2.5}$ over the PRD region of China are comparatively analyzed using two advanced source contribution modeling approaches: RSM and PSAT.
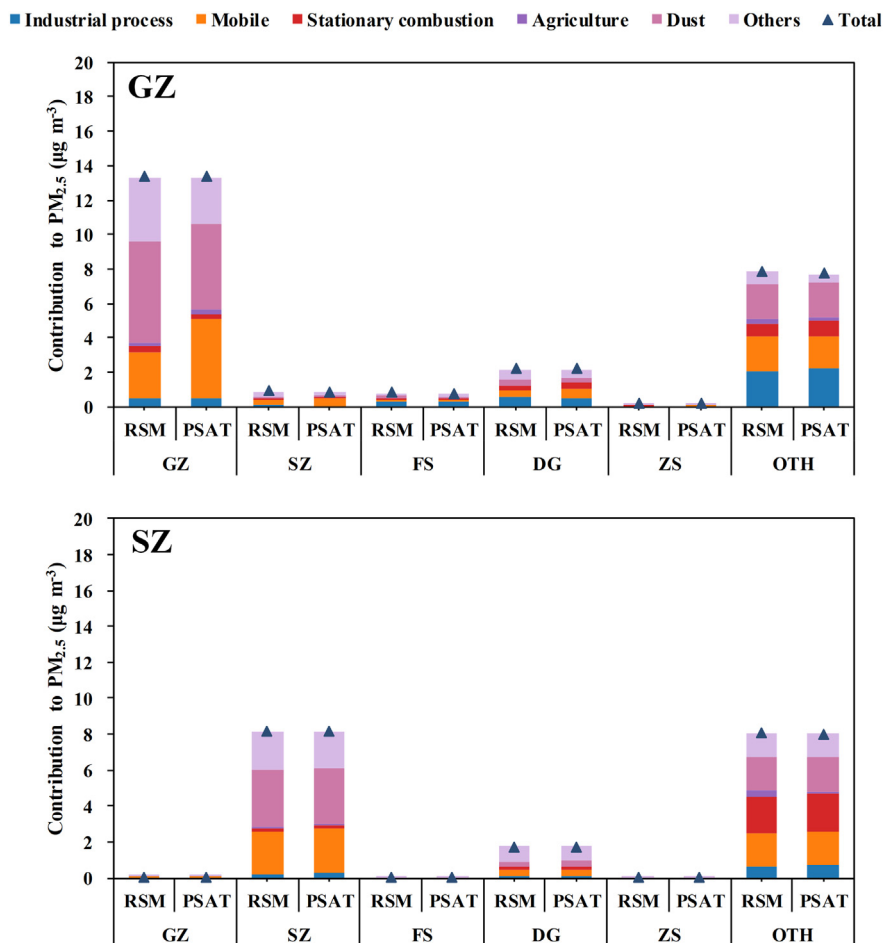

Fig. 6. Comparison of the contributions to monthly mean $PM_{2.5}$ concentrations in GZ and SZ from different source regions and sectors in January (RSM results are generated by a 100% reduction in all emissions; Blue triangle: total contribution of all sector emissions from each source region; GZ: Guangzhou, SZ: Shenzhen, FS: Foshan, DG: Dongguan, ZS: Zhongshan, OTH: all the other areas in the d03 domain). (For interpretation of the references to color in this figure legend, the reader is referred to the web version of this article.)

The comparative analyses show that both RSM and PSAT are capable of reasonably evaluating the contribution of primary $PM_{2.5}$ emission sources to ambient $PM_{2.5}$ because of its linear nature. However, they exhibit different performances in assessing the source contributions to secondary $PM_{2.5}$ formed by the nonlinear reactions among $PM_{2.5}$ precursors. PSAT seems to be limited by its capability in quantifying the nonlinear contribution of $PM_{2.5}$ precursors to emission changes, for example the $PM_{2.5}$ disbenefits due to local NO_x emission reductions in GZ and DG, because it assumes that each secondary $PM_{2.5}$ compound is attributed only to its direct primary precursor (e.g., the sulfate is only apportioned to SO_2, the nitrate to NO_x, and the ammonium to NH_3), but ignores the indirect effects caused by nonlinear interactions among precursors (e.g., the increase in sulfate concentrations resulting from a reduction in NO_x emissions). RSM is able to well identify the nonlinear relationship among $PM_{2.5}$ precursors and catch their nonlinear contributions to $PM_{2.5}$ as demonstrated in the PRD case.

The source contribution results illustrate that for the ambient $PM_{2.5}$ in the central cities (GZ, SZ, FS, DG, and ZS) of the PRD, the regional source emissions contribute the most by 42–66%; the dust emissions are the top contribution sources (29–34% by RSM and 27–31% by PSAT), and the mobile sources are ranked as the secondary contributors accounting for 16–25% by RSM and 19–30% by PSAT among the anthropogenic emission sources. Accordingly, to effectively lower the ambient $PM_{2.5}$ concentration in the PRD, the city-scale cooperation on emission reductions and the strengthening of dust and mobile source control are suggested.

The establishment of RSM requires hundreds of simulations, but once built, it can achieve the real-time source contribution analysis under different emission control scenarios. It is because RSM can rapidly repeat the source apportionment results generated from brute force scenarios that can directly be explained by emission reductions. PSAT only needs one simulation for source apportionment analysis of one scenario, but its results only represent the specific emission scenario that is simulated and cannot be interpreted in terms of different emission reductions. Therefore, PSAT may be inefficient if applied to different emission scenarios, because the computational time required for PSAT will increase significantly when there are a huge number of emission reduction scenarios to be simulated. Maintaining a high predictive performance while reducing the required computational cost has always been our goal for RSM development. With the continuous improvement of RSM, the computational resource consumption required for RSM construction has been greatly reduced, and even only two simulations can be used to successfully create an efficient RSM through the machine learning technology (Xing et al., 2020b). The combination of source contribution analysis with the latest low computational burden RSM has been listed in our next step development plan.

CRediT authorship contribution statement

Zhifang Li: Conceptualization, Methodology, Software, Investigation, Writing – original draft. **Yun Zhu:** Resources, Writing – review & editing, Supervision, Project administration, Data curation. **Shuxiao Wang:** Resources, Writing – review & editing, Data curation. **Jia Xing:** Resources, Writing – review & editing, Data curation. **Bin Zhao:** Writing – review & editing. **Shicheng Long:** Writing – review & editing. **Minhui Li:** Writing – review & editing. **Wenwei Yang:** Validation, Formal analysis, Visualization, Software. **Ruolin Huang:** Validation, Formal analysis, Visualization, Software. **Ying Chen:** Validation, Formal analysis, Visualization.

Declaration of competing interest

The authors declare that they have no known competing financial interests or personal relationships that could have appeared to influence the work reported in this paper.

Appendix A. Supplementary data

Supplementary data to this article can be found online at https://doi.org/10.1016/j.scitotenv.2021.151757.

References

Belis, C.A., Karagulian, F., Larsen, B.R., Hopke, P.K., 2013. Critical review and meta-analysis of ambient particulate matter source apportionment using receptor models in Europe. Atmos. Environ. 69, 94–108. https://doi.org/10.1016/j.atmosenv.2012.11.009.

Bi, X.H., Feng, Y.C., Zhu, T., Zhang, Y.F., Wu, J.H., Li, X., 2011. Determination of buffering capacity of total suspended particle and its source apportionment using the chemical mass balance approach. J. Air Waste Manag. Assoc. 61, 7–13. https://doi.org/10.3155/1047-3289.61.1.7.

Burr, M.J., Zhang, Y., 2011a. Source apportionment of fine particulate matter over the eastern U.S. Part I: source sensitivity simulations using CMAQ with the brute force method. Atmos. Pollut. Res. 2, 300–317. https://doi.org/10.5094/Apr.2011.036.

Burr, M.J., Zhang, Y., 2011b. Source apportionment of fine particulate matter over the eastern U.S. Part II: source apportionment simulations using CAMx/PSAT and comparisons with CMAQ source sensitivity simulations. Atmos. Pollut. Res. 2, 318–336. https://doi.org/10.5094/Apr.2011.037.

Byun, D., Schere, K.L., 2006. Review of the governing equations, computational algorithms, and other components of the models-3 community multiscale air quality (CMAQ) modeling system. Appl. Mech. Rev. 59, 51–77. https://doi.org/10.1115/1.2128636.

Chang, X., Wang, S.X., Zhao, B., Xing, J., Liu, X.X., Wei, L., Song, Y., Wu, W.J., Cai, S.Y., Zheng, H.T., Ding, D., Zheng, M., 2019. Contributions of inter-city and regional transport to PM2.5 concentrations in the Beijing-Tianjin-Hebei region and its implications on regional joint air pollution control. Sci. Total Environ. 660, 1191–1200. https://doi.org/10.1016/j.scitotenv.2018.12.474.

Chatani, S., Shimadera, H., Itahashi, S., Yamaji, K., 2020. Comprehensive analyses of source sensitivities and apportionments of PM2.5 and ozone over Japan via multiple numerical techniques. Atmos. Chem. Phys. 20, 10311–10329. https://doi.org/10.5194/acp-20-10311-2020.

Chen, D.S., Liu, X.X., Lang, J.L., Zhou, Y., Wei, L., Wang, X.T., Guo, X.R., 2017. Estimating the contribution of regional transport to PM2.5 air pollution in a rural area on the North China plain. Sci. Total Environ. 583, 280–291. https://doi.org/10.1016/j.scitotenv.2017.01.066.

Chen, D.S., Zhao, N., Lang, J.L., Zhou, Y., Wang, X.T., Li, Y., Zhao, Y.H., Guo, X.R., 2018. Contribution of ship emissions to the concentration of PM2.5: a comprehensive study using AIS data and WRF/Chem model in Bohai Rim Region, China. Sci. Total Environ. 610–611, 1476–1486. https://doi.org/10.1016/j.scitotenv.2017.07.255.

Chen, Y., Fung, J.C.H., Chen, D.H., Shen, J., Lu, X.C., 2019. Source and exposure apportionments of ambient PM2.5 under different synoptic patterns in the Pearl River Delta region. Chemosphere 236, 124266. https://doi.org/10.1016/j.chemosphere.2019.06.236.

China, S.C., 2021. The anouncement of the 14th Five-Year Plan. http://www.gov.cn/xinwen/2021-03/13/content_5592681.htm (accessed 19 May 2021).(in Chinese).

Clappier, A., Belis, C.A., Pernigotti, D., Thunis, P., 2017. Source apportionment and sensitivity analysis: two methodologies with two different purposes. Geosci. Model Dev. 10, 4245–4256. https://doi.org/10.5194/gmd-10-4245-2017.

Cohan, D.S., Hakami, A., Hu, Y., Russell, A.G., 2005. Nonlinear response of ozone to emissions: source apportionment and sensitivity analysis. Environ. Sci. Technol. 39, 6739–6748. https://doi.org/10.1021/es048664m.

Dunker, A.M., 1984. The decoupled direct method for calculating sensitivity coefficients in chemical kinetics. J. Chem. Phys. 81, 2385–2393. https://doi.org/10.1063/1.447938.

Dunker, A.M., Yarwood, G., Ortmann, J.P., Wilson, G.M., 2002. Comparison of source apportionment and source sensitivity of ozone in a three-dimensional air quality model. Environ. Sci. Technol. 36, 2953–2964. https://doi.org/10.1021/es011418f.

Emery, C., Liu, Z., Russell, A.G., Odman, M.T., Yarwood, G., Kumar, N., 2017. Recommendations on statistics and benchmarks to assess photochemical model performance. J. Air Waste Manage. Assoc. 67, 582–598. https://doi.org/10.1080/10962247.2016.1265027.

Fang, T.T., Zhu, Y., Jang, J.C., Wang, S.X., Xing, J., Chiang, P.C., Fan, S.J., You, Z.Q., Li, J.Y., 2020. Real-time source contribution analysis of ambient ozone using an enhanced meta-modeling approach over the Pearl River Delta region of China. J. Environ. Manag. 268, 110650. https://doi.org/10.1016/j.jenvman.2020.110650.

Fang, T.T., Zhu, Y., Wang, S.X., Xing, J., Zhao, B., Fan, S.J., Li, M.H., Yang, W.W., Chen, Y., Huang, R.L., 2021. Source impact and contribution analysis of ambient ozone using multi-modeling approaches over the Pearl River Delta region, China. Environ. Pollut. 289, 117860. https://doi.org/10.1016/j.envpol.2021.117860.

Foley, K.M., Roselle, S.J., Appel, K.W., Bhave, P.V., Pleim, J.E., Otte, T.L., Mathur, R., Sarwar, G., Young, J.O., Gilliam, R.C., Nolte, C.G., Kelly, J.T., Gilliland, A.B., Bash, J.O., 2010. Incremental testing of the community multiscale air quality (CMAQ) modeling system version 4.7. Geosci. Model Dev. 3, 205–226. https://doi.org/10.5194/gmd-3-205-2010.

Foley, K.M., Napelenok, S.L., Jang, C., Phillips, S., Hubbell, B.J., Fulcher, C.M., 2014. Two reduced form air quality modeling techniques for rapidly calculating pollutant mitigation potential across many sources, locations and precursor emission types. Atmos. Environ. 98, 283–289. https://doi.org/10.1016/j.atmosenv.2014.08.046.

Fu, X., Wang, S.X., Xing, J., Zhang, X.Y., Wang, T., Hao, J.M., 2017. Increasing ammonia concentrations reduce the effectiveness of particle pollution control achieved via SO2 and NOX emissions reduction in East China. Environ. Sci. Technol. Lett. 4, 221–227. https://doi.org/10.1021/acs.estlett.7b00143.

GDEEP, 2021. 2020 report on the state of Guangdong provincial environment. http://gdee.gd.gov.cn/hjzkgb/content/post_3266052.html (accessed 19 May 2021).(in Chinese).

Guenther, A.B., Jiang, X., Heald, C.L., Sakulyanontvittaya, T., Duhl, T., Emmons, L.K., Wang, X., 2012. The model of emissions of gases and aerosols from nature version 2.1 (MEGAN2.1): an extended and updated framework for modeling biogenic emissions. Geosci. Model Dev. 5, 1471–1492. https://doi.org/10.5194/gmd-5-1471-2012.

Hakami, A., Odman, M.T., Russell, A.G., 2003. High-order, direct sensitivity analysis of multidimensional air quality models. Environ. Sci. Technol. 37, 2442–2452. https://doi.org/10.1021/es020677h.

Hakami, A., Odman, M.T., Russell, A.G., 2004. Nonlinearity in atmospheric response: a direct sensitivity analysis approach. J. Geophys. Res. Atmos. 109. https://doi.org/10.1029/2003JD004502.

HKEPD, 2018. Pearl River Delta regional air quality monitoring report. https://www.epd.gov.hk/epd/sites/default/files/epd/english/resources_pub/publications/files/PRD_2017_report_en.pdf (accessed 19 May 2021).

Huang, Y.Q., Deng, T., Li, Z.N., Wang, N., Yin, C.Q., Wang, S.Q., Fan, S.J., 2018. Numerical simulations for the sources apportionment and control strategies of PM2.5 over Pearl River Delta, China, part I: inventory and PM2.5 sources apportionment. Sci. Total Environ. 634, 1631–1644. https://doi.org/10.1016/j.scitotenv.2018.04.208.

Huang, J.Y., Zhu, Y., Kelly, J.T., Jang, C., Wang, S.X., Xing, J., Chiang, P.C., Fan, S.J., Zhao, X.T., Yu, L., 2020. Large-scale optimization of multi-pollutant control strategies in the Pearl River Delta region of China using a genetic algorithm in machine learning. Sci. Total Environ. 722, 137701. https://doi.org/10.1016/j.scitotenv.2020.137701.

Itahashi, S., Hayami, H., Uno, I., 2015. Comprehensive study of emission source contributions for tropospheric ozone formation over East Asia. J. Geophys. Res.-Atmos. 120, 331–358. https://doi.org/10.1002/2014jd022117.

Itahashi, S., Hayami, H., Yumimoto, K., Uno, I., 2017. Chinese province-scale source apportionments for sulfate aerosol in 2005 evaluated by the tagged tracer method. Environ. Pollut. 220, 1366–1375. https://doi.org/10.1016/j.envpol.2016.10.098.

Ivey, C.E., Holmes, H.A., Hu, Y.T., Mulholland, J.A., Russell, A.G., 2015. Development of PM2.5 source impact spatial fields using a hybrid source apportionment air quality model. Geosci. Model Dev. 8, 2153–2165. https://doi.org/10.5194/gmd-8-2153-2015.

Jiménez, P.A., Dudhia, J., 2012. Improving the representation of resolved and unresolved topographic effects on surface wind in the WRF model. J. Appl. Meteorol. Climatol. 51, 300–316. https://doi.org/10.1175/JAMC-D-11-084.1.

Jin, J.B., Zhu, Y., Jang, J.C., Wang, S.X., Xing, J., Chiang, P.C., Fan, S.J., Long, S.C., 2020. Enhancement of the polynomial functions response surface model for real-time analyzing ozone sensitivity. Front. Env. Sci. Eng. 15, 31. https://doi.org/10.1007/s11783-020-1323-0.

Kim, B.U., Bae, C., Kim, H.C., Kim, E., Kim, S., 2017. Spatially and chemically resolved source apportionment analysis: case study of high particulate matter event. Atmos. Environ. 162, 55–70. https://doi.org/10.1016/j.atmosenv.2017.05.006.

Koo, B., Wilson, G.M., Morris, R.E., Dunker, A.M., Yarwood, G., 2009. Comparison of source apportionment and sensitivity analysis in a particulate matter air quality model. Environ. Sci. Technol. 43, 6669–6675. https://doi.org/10.1021/es9008129.

Kranenburg, R., Segers, A.J., Hendriks, C., Schaap, M., 2013. Source apportionment using LOTOS-EUROS: module description and evaluation. Geosci. Model Dev. 6, 721–733. https://doi.org/10.5194/gmd-6-721-2013.

Li, X., Zhang, Q., Zhang, Y., Zheng, B., Wang, K., Chen, Y., Wallington, T.J., Han, W.J., Shen, W., Zhang, X.Y., He, K.B., 2015. Source contributions of urban PM2.5 in the Beijing–Tianjin–Hebei region: changes between 2006 and 2013 and relative impacts of emissions and meteorology. Atmos. Environ. 123, 229–239. https://doi.org/10.1016/j.atmosenv.2015.10.048.

Li, L., An, J.Y., Zhou, M., Qiao, L.P., Zhu, S.H., Yan, R.S., Ooi, C.G., Wang, H.L., Huang, C., Huang, L., Tao, S.K., Yu, J.Z., Chan, A., Wang, Y.J., Feng, J.L., Chen, C.H., 2018. An integrated source apportionment methodology and its application over the Yangtze River Delta region, China. Environ. Sci. Technol. 52, 14216–14227. https://doi.org/10.1021/acs.est.8b01211.

Liu, X.Y., Bai, X.X., Tian, H.Z., Wang, K., Hua, S.B., Liu, H.J., Liu, S.H., Wu, B.B., Wu, Y.M., Liu, W., Luo, L.N., Wang, Y.X., Hao, J.M., Lin, S.M., Zhao, S., Zhang, K., 2020. Fine particulate matter pollution in North China: seasonal-spatial variations, source apportionment, sector and regional transport contributions. Environ. Res. 184, 109368. https://doi.org/10.1016/j.envres.2020.109368.

Long, S.C., Zhu, Y., Jang, C., Lin, C.J., Wang, S.X., Zhao, B., Gao, J., Deng, S., Xie, J.P., Qiu, X.Z., 2016. A case study of development and application of a streamlined control and response modeling system for PM2.5 attainment assessment in China. J. Environ. Sci.-China 41, 69–80. https://doi.org/10.1016/j.jes.2015.05.019.

Lu, X.C., Chen, Y., Huang, Y.Q., Lin, C.Q., Li, Z.Y., Fung, J.C.H., Lau, A.K.H., 2019. Differences in concentration and source apportionment of PM2.5 between 2006 and 2015 over the PRD region in southern China. Sci. Total Environ. 673, 708–718. https://doi.org/10.1016/j.scitotenv.2019.03.452.

Napelenok, S.L., Vedantham, R., Bhave, P.V., Pouliot, G.A., Kwok, R.H.F., 2014. Source-receptor reconciliation of fine-particulate emissions from residential wood combustion in the southeastern United States. Atmos. Environ. 98, 454–460. https://doi.org/10.1016/j.atmosenv.2014.09.021.

Paatero, P., Tapper, U., 1994. Positive matrix factorization: a non-negative factor model with optimal utilization of error estimates of data values. Environmetrics 5, 111–126. https://doi.org/10.1002/env.3170050203.

Pan, Y.Z., Zhu, Y., Jang, J.C., Wang, S.X., Xing, J., Chiang, P.C., Zhao, X.T., You, Z.Q., Yuan, Y.Z., 2020. Source and sectoral contribution analysis of PM2.5 based on efficient response surface modeling technique over Pearl River Delta region of China. Sci. Total Environ. 737, 139655. https://doi.org/10.1016/j.scitotenv.2020.139655.

Santos-Alamillos, F.J., Pozo-Vázquez, D., Ruiz-Arias, J.A., Tovar-Pescador, J., 2015. Influence of land-use misrepresentation on the accuracy of WRF wind estimates: evaluation of GLCC and CORINE land-use maps in southern Spain. Atmos. Res. 157, 17–28. https://doi.org/10.1016/j.atmosres.2015.01.006.

Thunis, P., Degraeuwe, B., Pisoni, E., Trombetti, M., Peduzzi, E., Belis, C.A., Wilson, J., Clappier, A., Vignati, E., 2018. PM2.5 source allocation in european cities: a SHERPA modelling study. Atmos. Environ. 187, 93–106. https://doi.org/10.1016/j.atmosenv.2018.05.062.

Thunis, P., Clappier, A., Tarrason, L., Cuvelier, C., Monteiro, A., Pisoni, E., Wesseling, J., Belis, C.A., Pirovano, G., Janssen, S., Guerreiro, C., Peduzzi, E., 2019. Source apportionment to support air quality planning: strengths and weaknesses of existing approaches. Environ. Int. 130, 104825. https://doi.org/10.1016/j.envint.2019.05.019.

Thunis, P., Clappier, A., Beekmann, M., Putaud, J.P., Cuvelier, C., Madrazo, J., de Meij, A., 2021. Non-linear response of PM2.5 to changes in NOx and NH3 emissions in the Po basin (Italy): consequences for air quality plans. Atmos. Chem. Phys. 21, 9309–9327. https://doi.org/10.5194/acp-21-9309-2021.

Wang, X.F., Zhang, Y.P., Chen, H., Yang, X., Chen, J.M., Geng, F.H., 2009. Particulate nitrate formation in a highly polluted urban area: a case study by single-particle mass spectrometry in Shanghai. Environ. Sci. Technol. 43, 3061–3066. https://doi.org/10.1021/es8020155.

Wang, S.X., Xing, J., Jang, C., Zhu, Y., Fu, J.S., Hao, J.M., 2011. Impact assessment of ammonia emissions on inorganic aerosols in East China using response surface modeling technique. Environ. Sci. Technol. 45, 9293–9300. https://doi.org/10.1021/es2022347.

Wang, G., Cheng, S.Y., Wei, W., Zhou, Y., Yao, S., Zhang, H.Y., 2016. Characteristics and source apportionment of VOCs in the suburban area of Beijing China. Atmos. Pollut. Res. 7, 711–724. https://doi.org/10.1016/j.apr.2016.03.006.

Wang, Y.J., Bao, S.W., Wang, S.X., Hu, Y.T., Shi, X., Wang, J.D., Zhao, B., Jiang, J.K., Zheng, M., Wu, M.H., Russell, A.G., Wang, Y.H., Hao, J.M., 2017. Local and regional contributions to fine particulate matter in Beijing during heavy haze episodes. Sci. Total Environ. 580, 283–296. https://doi.org/10.1016/j.scitotenv.2016.12.127.

Watson, J.G., Cooper, J.A., Huntzicker, J.J., 1984. The effective variance weighting for least squares calculations applied to the mass balance receptor model. Atmos. Environ. 18, 1347–1355. https://doi.org/10.1016/0004-6981(84)90043-X.

Wu, D.W., Fung, J.C.H., Yao, T., Lau, A.K.H., 2013. A study of control policy in the Pearl River Delta region by using the particulate matter source apportionment method. Atmos. Environ. 76, 147–161. https://doi.org/10.1016/j.atmosenv.2012.11.069.

Xie, M., Zhu, K.G., Wang, T.J., Feng, W., Gao, D., Li, M.M., Li, S., Zhuang, B.L., Han, Y., Chen, P.L., Liao, J.B., 2016. Changes in regional meteorology induced by anthropogenic heat and their impacts on air quality in South China. Atmos. Chem. Phys. 16, 15011–15031. https://doi.org/10.5194/acp-16-15011-2016.

Xing, J., Wang, S.X., Jang, C., Zhu, Y., Hao, J.M., 2011. Nonlinear response of ozone to precursor emission changes in China: a modeling study using response surface methodology. Atmos. Chem. Phys. 11, 5027–5044. https://doi.org/10.5194/acp-11-5027-2011.

Xing, J., Wang, S.X., Zhao, B., Wu, W.J., Ding, D., Jang, C., Zhu, Y., Chang, X., Wang, J.D., Zhang, F.F., Hao, J.M., 2017. Quantifying nonlinear multiregional contributions to ozone and fine particles using an updated response surface modeling technique. Environ. Sci. Technol. 51, 11788–11798. https://doi.org/10.1021/acs.est.7b01975.

Xing, J., Ding, D., Wang, S.X., Zhao, B., Jang, C., Wu, W.J., Zhang, F.F., Zhu, Y., Hao, J.M., 2018. Quantification of the enhanced effectiveness of NOx control from simultaneous reductions of VOC and NH3 for reducing air pollution in the Beijing–Tianjin–Hebei region, China. Atmos. Chem. Phys. 18, 7799–7814. https://doi.org/10.5194/acp-18-7799-2018.

Xing, J., Ding, D., Wang, S.X., Dong, Z.X., Kelly, J.T., Jang, C., Zhu, Y., Hao, J.M., 2019. Development and application of observable response indicators for design of an effective ozone and fine-particle pollution control strategy in China. Atmos. Chem. Phys. 19, 13627–13646. https://doi.org/10.5194/acp-19-13627-2019.

Xing, J., Li, S.W., Jiang, Y.Q., Wang, S.X., Ding, D., Dong, Z.X., Zhu, Y., Hao, J.M., 2020a. Quantifying the emission changes and associated air quality impacts during the COVID-19 pandemic on the North China plain: a response modeling study. Atmos. Chem. Phys. 20, 14347–14359. https://doi.org/10.5194/acp-20-14347-2020.

Xing, J., Zheng, S.X., Ding, D., Kelly, J.T., Wang, S.X., Li, S.W., Qin, T., Ma, M.Y., Dong, Z.X., Jang, C., Zhu, Y., Zheng, H.T., Ren, L., Liu, T.Y., Hao, J.M., 2020b. Deep learning for prediction of the air quality response to emission changes. Environ. Sci. Technol. 54, 8589–8600. https://doi.org/10.1021/acs.est.0c02923.

Yamaji, K., Uno, I., Irie, H., 2012. Investigating the response of east asian ozone to chinese emission changes using a linear approach. Atmos. Environ. 55, 475–482. https://doi.org/10.1016/j.atmosenv.2012.03.009.

Yang, W.Y., Chen, H.S., Wu, J.B., Wang, W.D., Zheng, J.Y., Chen, D.H., Li, J., Tang, X., Wang, Z.F., Zhu, L.L., Wang, W., 2020. Characteristics of the source apportionment of primary and secondary inorganic PM2.5 in the Pearl River Delta region during 2015 by numerical modeling. Environ. Pollut. 267, 115418. https://doi.org/10.1016/j.envpol.2020.115418.

Yin, X.H., Huang, Z.J., Zheng, J.Y., Yuan, Z.B., Zhu, W.B., Huang, X.B., Chen, D.H., 2017. Source contributions to PM2.5 in Guangdong province, China by numerical modeling:

results and implications. Atmos. Res. 186, 63–71. https://doi.org/10.1016/j.atmosres.2016.11.007.

Yin, S.S., Huang, Z.J., Zheng, J.Y., Huang, X.B., Chen, D.H., Tan, H.B., 2018. Characteristics of inorganic aerosol formation over ammonia-poor and ammonia-rich areas in the Pearl River Delta region, China. Atmos. Environ. 177, 120–131. https://doi.org/10.1016/j.atmosenv.2018.01.005.

Zhang, Y., Vijayaraghavan, K., Seigneur, C., 2005. Evaluation of three probing techniques in a three-dimensional air quality model. J. Geophys. Res. 110. https://doi.org/10.1029/2004jd005248.

Zhang, Y.J., Cai, J., Wang, S.X., He, K.B., Zheng, M., 2017. Review of receptor-based source apportionment research of fine particulate matter and its challenges in China. Sci. Total Environ. 586, 917–929. https://doi.org/10.1016/j.scitotenv.2017.02.071.

Zhao, B., Wang, S.X., Xing, J., Fu, K., Fu, J.S., Jang, C., Zhu, Y., Dong, X.Y., Gao, Y., Wu, W.J., Wang, J.D., Hao, J.M., 2015. Assessing the nonlinear response of fine particles to precursor emissions: development and application of an extended response surface

modeling technique v1.0. Geosci. Model Dev. 8, 115–128. https://doi.org/10.5194/gmd-8-115-2015.

Zhao, B., Wu, W.J., Wang, S.X., Xing, J., Chang, X., Liou, K.N., Jiang, J.H., Gu, Y., Jang, C., Fu, J.S., Zhu, Y., Wang, J.D., Lin, Y., Hao, J.M., 2017. A modeling study of the nonlinear response of fine particles to air pollutant emissions in the Beijing–Tianjin–Hebei region. Atmos. Chem. Phys. 17, 12031–12050. https://doi.org/10.5194/acp-17-12031-2017.

Zheng, B., Tong, D., Li, M., Liu, F., Hong, C.P., Geng, G.N., Li, H.Y., Li, X., Peng, L.Q., Qi, J., Yan, L., Zhang, Y.X., Zhao, H.Y., Zheng, Y.X., He, K.B., Zhang, Q., 2018. Trends in China's anthropogenic emissions since 2010 as the consequence of clean air actions. Atmos. Chem. Phys. 18, 14095–14111. https://doi.org/10.5194/acp-18-14095-2018.

Zhu, Y.H., Huang, L., Li, J.Y., Ying, Q., Zhang, H.L., Liu, X.G., Liao, H., Li, N., Liu, Z.X., Mao, Y.H., Fang, H., Hu, J.L., 2018. Sources of particulate matter in China: insights from source apportionment studies published in 1987–2017. Environ. Int. 115, 343–357. https://doi.org/10.1016/j.envint.2018.03.037.